IOP Publishing | International Atomic Energy Agency Nuclear Fusion
Nucl. Fusion **00** (2017) 000000 (9pp) UNCORRECTED PROOF

Role of a continuous MHD dynamo in the formation of 3D equilibria in fusion plasmas

P. Piovesan[1], D. Bonfiglio[1], M. Cianciosa[2], T.C. Luce[3], N.Z. Taylor[4], D. Terranova[1], F. Turco[5], R.S. Wilcox[2], A. Wingen[2], S. Cappello[1], C. Chrystal[3], D.F. Escande[6], C.T. Holcomb[7], L. Marrelli[1], C. Paz-Soldan[3], L. Piron[8], I. Predebon[1], B. Zaniol[1], The DIII-D and RFX-Mod Teams

[1] Consorzio RFX (CNR, ENEA, INFN, Università di Padova, Acciaierie Venete SpA), Corso Stati Uniti 4, 35127 Padova, Italy
[2] Oak Ridge National Laboratory, Oak Ridge, TN 37831, United States of America
[3] General Atomics, San Diego, CA 92186-5608, United States of America
[4] Oak Ridge Associated Universities, Oak Ridge, TN 37831, United States of America
[5] Department of Applied Physics and Applied Mathematics, Columbia University, New York, NY 10027, United States of America
[6] Aix-Marseille Université, CNRS, PIIM, UMR 7345, 13013 Marseille, France
[7] Lawrence Livermore National Laboratory, Livermore, CA 94550, United States of America
[8] CCFE, Culham Science Centre, Abingdon, OX14 3DB, United Kingdom AQ1

E-mail: paolo.piovesan@igi.cnr.it

Received 19 December 2016, revised 24 March 2017
Accepted for publication 28 April 2017
Published

Abstract

Stationary 3D equilibria can form in fusion plasmas via saturation of magnetohydrodynamic (MHD) instabilities or stimulated by external 3D fields. In these cases the current profile is anomalously broad due to magnetic flux pumping produced by the MHD modes. Flux pumping plays an important role in hybrid tokamak plasmas, maintaining the minimum safety factor above unity and thus removing sawteeth. It also enables steady-state hybrid operation, by redistributing non-inductive current driven near the center by electron cyclotron waves. A validated flux pumping model is not yet available, but it would be necessary to extrapolate hybrid operation to future devices. In this work flux pumping physics is investigated for helical core equilibria stimulated by external 3D fields in DIII-D hybrid plasmas. We show that flux pumping can be produced in a continuous way by an MHD dynamo emf. The same effect maintains helical equilibria in reversed-field pinch (RFP) plasmas. The effective MHD dynamo loop voltage is calculated for experimental 3D equilibrium reconstructions, by balancing Ohm's law over helical flux surfaces, and is consistent with the expected current redistribution. Similar results are also obtained with more sophisticated nonlinear MHD simulations. The same modelling approach is applied to helical RFP states forming spontaneously in RFX-mod as the plasma current is raised above 0.8–1 MA. This comparison allows to identify the underlying physics common to tokamak and RFP: a helical core displacement modulates parallel current density along flux tubes, which requires a helical electrostatic potential to build up, giving rise to a helical MHD dynamo flow.

Keywords: 3D equilibrium reconstruction, MHD dynamo, hybrid tokamak scenario, helical RFP states

AQ2 (Some figures may appear in colour only in the online journal) AQ3

JNL:NF PIPS: AA700B TYPE: PAP TS: NEWGEN DATE:8/5/17 EDITOR: IOP SPELLING: UK

1. Introduction

The confinement and stability properties of fusion plasmas are determined by various macroscopic quantities, among which an important role is played by the current density profile. Tailoring its shape with external actuators, for example neutral beam injection (NBI) and radio-frequency waves, is thus important to optimize high-performance operational scenarios. Broadening the current profile can stabilize deleterious magnetohydrodynamic (MHD) modes by reducing a source of free energy or by removing altogether their resonance, if the safety factor profile is elevated above low-order rational values, $q > m/n$, where m and n are the poloidal and toroidal mode numbers.

The MHD modes themselves can cause significant current redistribution. This effect is exploited in tokamaks operated in the so-called hybrid scenario [1–6]. Benign MHD modes saturated at modest amplitude redistribute central current in hybrid plasmas, thus keeping the minimum safety factor above unity, an effect known as poloidal magnetic flux pumping [7]. This removes sawteeth and makes in general $n = 1$ modes more stable, which allows to increase the normalized plasma pressure, $\beta_N = \beta_T a B_T / I_P$, up to about 3.5, well above the values typical of H-mode operation, $\beta_N \sim 2$ (here a is the minor radius, B_T the toroidal magnetic field and I_P the plasma current). Flux pumping is usually produced in the DIII-D tokamak by 3/2 or 4/3 tearing modes [7], while ASDEX Upgrade documented a similar effect either from 1/1 fishbones [8] or tearing modes [9].

Flux pumping is also important to enable steady-state hybrid operation in DIII-D, by efficiently redistributing significant amounts of non-inductive current driven by electron cyclotron waves near the plasma center, where this current drive method is most efficient [10, 11]. Various theories have been proposed to explain flux pumping in hybrid tokamak plasmas, but no validated model exists yet [12–14]. Such a model would be necessary to understand hybrid operation and to robustly extrapolate it to future devices like ITER.

In the present work, predictions of the MHD dynamo model of flux pumping are compared against experiments in DIII-D hybrid tokamak plasmas and in the RFX-mod reversed-field pinch (RFP). In both cases a stationary 3D equilibrium forms through the nonlinear saturation of an MHD mode, in a spontaneous way or stimulated by 3D fields externally applied by non-axisymmetric coils. In DIII-D a helical core equilibrium with dominant 1/1 harmonic forms stimulated by an external $n = 1$ field, due to the response of a kink mode that becomes marginally-stable at high β_N. Helical core states stimulated by external 3D fields were also obtained recently in ASDEX Upgrade [15]. These states share interesting similarities with the so-called $n = 1$ Long Lived Mode observed to form in the MAST spherical tokamak and modelled as a 3D equilibrium state in [16–18]. The helical state observed in RFPs, called quasi-single helicity (QSH), forms spontaneously as the plasma current is increased above 0.8–1 MA and is due to the saturation of a current-driven $m/n = 1/7$ kink-tearing mode [19], though this transition can also be stimulated by external 3D fields [20]. These two examples come from quite different magnetic configurations, but they share interesting commonalities, like the presence of a long-lasting helical core equilibrium and a possible role of an MHD dynamo in redistributing central current. These two aspects will be compared along the paper using similar analysis and modelling approaches.

The MHD dynamo model, largely developed for astrophysical plasmas [21–23], was applied for the first time in the fusion context to RFP plasmas [24], where it had several experimental confirmations [25–28]. Similar dynamo effects were also investigated in spheromaks [29, 30]. According to the single-fluid MHD dynamo model, an electromotive force (emf) is induced by flow and magnetic field fluctuations due to a turbulent spectrum of MHD modes via the $\langle \tilde{\mathbf{v}} \times \tilde{\mathbf{b}} \rangle$ term in Ohm's law, where $\langle \ldots \rangle$ represents an average over axisymmetric flux surfaces. When QSH states were observed in high-current RFP operation, the MHD dynamo produced by a single saturated mode was modelled with nonlinear MHD simulations [31–33] and compared with experiment [34, 35]. This allowed to gain significant insight in the basic physics mechanisms responsible for MHD dynamo in helical states, which remain valid also in other configurations.

The dynamo model mentioned above was developed based on nonlinear visco-resistive MHD simulations. They showed that the MHD dynamo emf in a stationary helical equilibrium is due to an electrostatic potential, φ, which forms to balance the modulation of parallel current density caused by the helical deformation of the flux surfaces [31–33]. Associated to this electrostatic potential, a helical flow is present, $\tilde{\mathbf{v}} = -\nabla\varphi \times \mathbf{B}/\mathbf{B}^2$, which produces a $\langle \tilde{\mathbf{v}} \times \tilde{\mathbf{b}} \rangle$ dynamo emf in a continuous way. The main results of this analysis are quite general and hold for any helical equilibrium resulting from the saturation of an MHD mode, as discussed in [33] (see in particular paragraph 2.1.1). The role of the dynamo electrostatic potential in the nonlinear saturation of the tearing mode has been discussed in [36]. The same dynamo effect has been recently proposed as a possible flux pumping mechanism to sustain high-β hybrid tokamak plasmas in [37], also based on nonlinear MHD simulations.

An interesting aspect of this model is worth being highlighted. Previous experimental work showed that in DIII-D hybrid plasmas flux pumping is mainly produced during transient events of coupling between the dominant tearing mode and edge-localized modes (ELMs) [7]. The important question thus arises whether flux pumping will work in fully stationary conditions, for example in plasmas with suppressed or no ELMs, as required in a fusion reactor, or if some temporal variation of the mode amplitude is necessary. The MHD dynamo model considered here predicts that flux pumping can work in a stationary way, with no need of transient events, a very promising feature in view of future tokamak operation.

This paper presents an attempt to validate the MHD dynamo model of flux pumping against experiments in different magnetic configurations. It will be shown in particular that the MHD dynamo emf can be directly calculated from a reconstruction of the experimental 3D equilibrium. This was obtained in RFP and tokamak plasmas using the V3FIT/VMEC code [38]

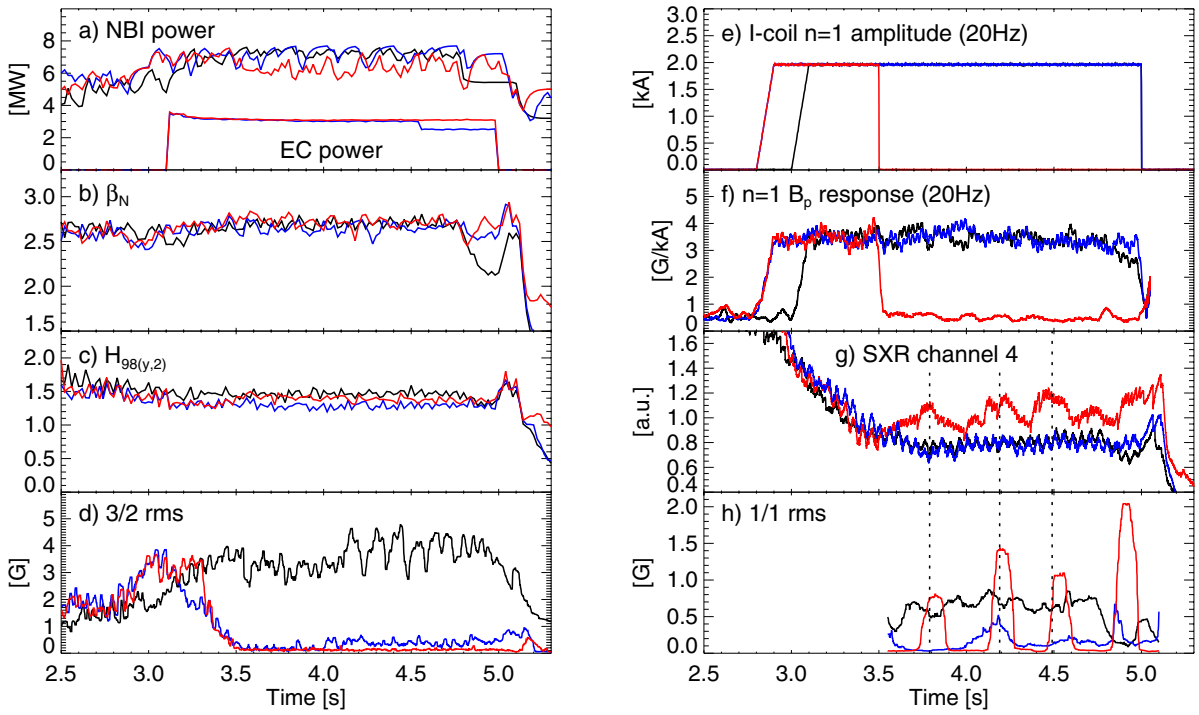

Figure 1. Main waveforms of three DIII-D hybrid discharges: (*a*) NBI and EC power, (*b*) normalized plasma pressure, (*c*) energy confinement enhancement factor, (*d*) rms of the 3/2 tearing mode, (*e*) $n = 1$ amplitude of the I-coil current, (*f*) $n = 1$ plasma response measured by a toroidal array of B_p magnetic probes on the outboard midplane, (*g*) SXR brightness measured by a central chord, and (*h*) rms of the fast rotating 1/1 mode. The black discharge has both a 3/2 mode and a helical core induced by the $n = 1$ applied field; the blue discharge has a long flattop with the 3/2 mode suppressed by ECCD and the helical core applied, while the red discharge has the 3/2 mode suppressed and no helical core.

constrained by internal measurements of the helical flux surface distortion. Section 2 presents a calculation of the dynamo emf for DIII-D hybrid plasmas with a helical core equilibrium stimulated by external 3D fields. Nonlinear MHD simulations of tokamak plasmas with saturated 1/1 and 2/1 modes are presented in section 3 and compared with previous similar work done for helical RFP states. Section 4 reports dynamo emf calculations for 3D equilibrium reconstructions of helical RFP plasmas in RFX-mod, which are analogous to those presented here for the DIII-D tokamak. Conclusions and future work are discussed in section 5.

2. Flux pumping by a helical core equilibrium in DIII-D hybrid plasmas

Recent DIII-D experiments investigated the physics of flux pumping in high-β hybrid plasmas exploiting a special property of the plasma response to externally applied $n = 1$ fields in this scenario. Due to the central safety factor lying just above unity, the $n = 1$ response profile is largely dominated by the core 1/1 harmonic of a marginally-stable kink mode, as found in ASDEX Upgrade and reproduced in DIII-D [15]. In other terms, the external $n = 1$ field stimulates the formation of a helical core equilibrium, with significant displacements of a few cm. The flux pumping produced by the helical core has been measured in experiment and compared to predictions of the MHD dynamo model, as it will be described in the following. These calculations were largely facilitated by the availability of a 3D equilibrium reconstruction of the helical core, recently obtained for the first time in a tokamak using the V3FIT/VMEC code [39, 40]. This allowed to calculate the MHD dynamo emf directly from the 3D equilibrium fitted in experiment, without going through more complicated nonlinear MHD simulations.

The DIII-D experiment is described in detail in figure 1, which reports three similar hybrid discharges. All cases have $\beta_N \simeq 2.7$ feedback controlled by regulating the NBI power, plasma current $I_P = 1.2$ MA and safety factor at the 95% magnetic flux surface $q_{95} = 4.2$. A helical core is induced during the flattop by applying an $n = 1$ field slowly-rotating at 20 Hz with internal non-axisymmetric coils (I-coils). The $n = 1$ response measured by poloidal field probes on the outboard midplane is shown in panel (*f*) and is quite constant throughout the flattop. The slow rotation is useful to detect the helical distortion with multiple diagnostics located at single toroidal positions. Pre-programmed $n = 1$ error field correction using a standard scheme is applied with external coils (C-coils). The I-coil perturbation causes an increased request of NBI power of about 20% to maintain β_N constant. The energy confinement is slightly degraded, as shown by the enhancement factor $H_{98(y,2)}$ in panel (*c*), but these plasmas maintain in any case good performance and this level of applied $n = 1$ field does not cause locked modes.

Flux pumping is typically produced in hybrid plasmas by a 3/2 tearing mode saturated at modest amplitude. This is also the case in the present experiment, as shown in panel (*d*). In the discharge shown in black, the 3/2 mode co-exists with the

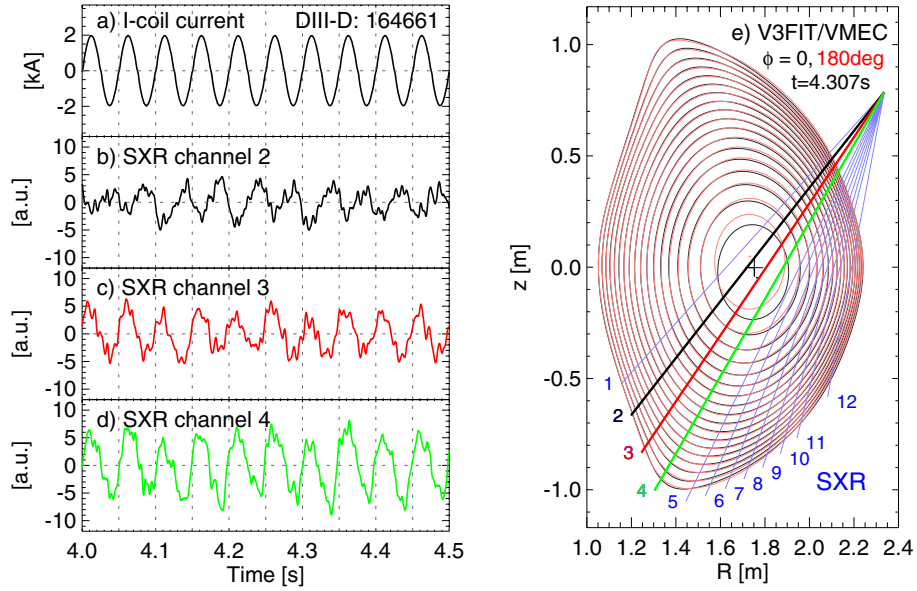

Figure 2. (*a*) I-coil current during a period with an $n = 1$ field applied rotating at 20 Hz in DIII-D discharge 164 661, also shown in figure 1. ((*b*)–(*d*)) SXR signals measured by the three chords marked respectively with black, red and green thick lines in panel (*d*). Panel (*d*) shows the helical flux surfaces reconstructed by the V3FIT/VMEC code at two toroidal angles 180° apart and the SXR chords used to constrain the 3D equilibrium fit.

externally-induced helical core. To isolate the flux pumping produced by the helical core alone, the 3/2 mode was suppressed by electron cyclotron current drive (ECCD) applied at its rational surface in the two discharges shown in red and blue. ECCD is applied at 3.1 s and the 3/2 amplitude decreases to almost zero in about 0.5 s. During this phase the $n = 1$ field is turned on, starting from 2.8 s. In the red case the $n = 1$ field is turned off again when the 3/2 is suppressed, while in the blue case it is kept for the entire flattop. In absence of both the 3/2 mode and the helical core (red case), $n = 1$ sawtooth-like activity is observed to come back, as shown by a soft x-ray (SXR) signal from a central chord in panel (*g*) and by the rms of the 1/1 fast rotating mode measured by a Mirnov coil in panel (*h*). This probably indicates a loss of hybrid conditions due to absence of flux pumping, as previously observed in [42]. On the other hand, no sawteeth are present when the helical core is induced and the 3/2 is suppressed (blue case). This indicates that the helical core alone may be able to sustain hybrid conditions by producing large enough flux pumping.

The level of flux pumping produced by the helical core was quantified using a technique developed in [43]. This approach uses several equilibrium reconstructions by the EFIT code during the entire discharge flattop to quantify the consumption inside the plasma of poloidal flux provided by external coils. In a recent work this method was applied to a wide database of DIII-D hybrid plasmas in different conditions, for example at different β_N values, showing that the poloidal flux is dissipated at a larger rate than it is supplied by the coils [44]. This poloidal flux deficit is shown to be proportional to the amount of flux pumping provided by the tearing mode. The same method was applied to the discharges of figure 1 and to other similar cases. Plasmas with an induced helical core and with the 3/2 mode suppressed have a finite poloidal flux deficit, systematically larger than cases without both the helical core and the 3/2 mode. The poloidal flux deficit corresponds to an effective loop voltage produced by the helical core that amounts to about −10 mV. The effective loop voltage is negative since it limits central current peaking by redistributing central current to larger radii. Similar values of poloidal flux deficit are obtained in the same type of hybrid discharges when the 3/2 mode is present and without the helical core.

A 3D equilibrium reconstruction of the helical core is necessary to calculate the MHD dynamo electric field. Such a reconstruction was provided by the V3FIT code [38], which begins with a kinetic EFIT solution and then iterates many VMEC runs trying to fit internal measurements of the 3D flux surface distortion. These are provided in the present experiments by a SXR diagnostic with 12 lines of sight over a poloidal cross-section and by a multi-channel Motional Stark Effect (MSE) diagnostic, giving thus information on both kinetic and magnetic field profiles. Figure 2 shows the resulting 3D equilibrium fit. A helical core distortion of about 4 cm is present, as evidenced by comparing two poloidal cuts of the helical flux surfaces at two toroidal angles 180° apart, shown in black and red respectively. The SXR signals measured by three central lines of sight passing on opposite sides of the magnetic axis are shown in panels (*b*) to (*c*). A 20 Hz oscillation in phase with the I-coil current is clearly present in all signals and is due to the fact that the $n = 1$ field is rotated in the toroidal direction. Oscillations in signals from opposite sides of the magnetic axis are out of phase, due to the dominant $m = 1$ distortion of the plasma core. More details on this 3D equilibrium fit will be described in a separate paper [40].

Time-dependent nonlinear MHD calculations are necessary to model the MHD dynamo self-consistently including its dynamics, the possible formation of magnetic islands and stochastic regions. The present work assumes that the helical core obtained in DIII-D can be represented by an ideal MHD

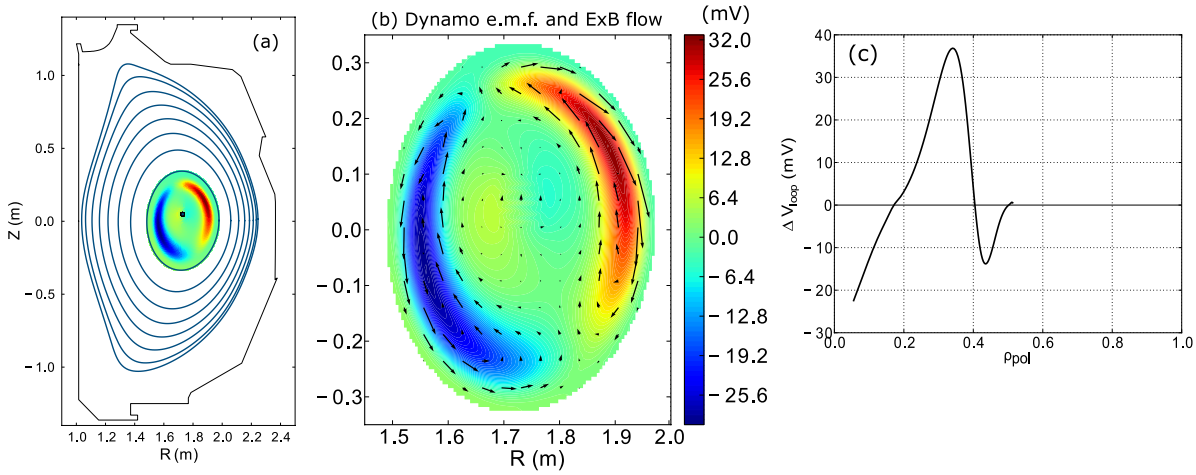

Figure 3. (*a*) Helical flux surfaces reconstructed by the V3FIT/VMEC code for DIII-D discharge 164 661 at $t = 4.307$ s, also described in figures 1 and 2. (*b*) Contour plot of the dynamo electrostatic potential predicted by balancing Ohm's law over the helical core equilibrium, as described in the text, and the associated $\mathbf{E} \times \mathbf{B}$ flow. (*c*) The effective dynamo loop voltage calculated by averaging the MHD dynamo electric field predicted for the helical core over axisymmetric flux surfaces.

3D equilibrium solution, such as the one provided by V3FIT/VMEC, even though it is important to keep in mind that this may not be a complete or fully self-consistent description of the plasma. Starting from this 3D equilibrium solution, the dynamo field has been calculated by balancing Ohm's law over the helical flux surfaces. Under stationary conditions $\nabla \times \mathbf{E} = 0$ and Ohm's law can be written as follows:

$$\mathbf{E}_{\rm loop} - \nabla\varphi = \eta_{\rm neo}(\mathbf{j} - \mathbf{j}_{\rm CD} - \mathbf{j}_{\rm BS}) - \mathbf{v} \times \mathbf{B} \quad (1)$$

$$= \eta_{\rm neo}\mathbf{j}_{\rm Ohm} - \mathbf{v} \times \mathbf{B} \quad (2)$$

where φ is the dynamo electrostatic potential, $\mathbf{j}$ the total current density from VMEC, $\mathbf{j}_{\rm CD}$ the externally driven current, which includes in the present experiments NBI and EC contributions, and $\mathbf{j}_{\rm BS}$ the bootstrap current. All these contributions can be separately calculated with dedicated codes. For example, in DIII-D the ONETWO transport code [41] and its modules were used. By projecting Ohm's law along the total magnetic field, $\mathbf{B}$, which includes here also helical perturbations, the following equation can be easily derived:

$$\frac{\mathbf{B}\cdot\nabla\varphi}{\mathbf{B}\cdot\nabla\theta} = \frac{\mathbf{B}\cdot(\mathbf{E}_{\rm loop} - \eta_{\rm neo}\mathbf{j}_{\rm Ohm})}{\mathbf{B}\cdot\nabla\theta} = \partial_\theta\varphi + q\partial_\zeta\varphi, \quad (3)$$

where θ and ζ are respectively the straight-field-line poloidal and toroidal angles. The only unknown is the electrostatic potential φ, while the other terms can be obtained from the 3D equilibrium reconstruction or they can be calculated from experimental data. Note that equation (3) was originally derived in [33] and is here generalized to straight-field-line coordinates. The dynamo potential can be thus obtained by integrating the above equation over helical flux surfaces. It is important to note that some approximations are made in this calculation. In particular, the current driven by NBI and ECCD and the bootstrap current are modelled by codes in 2D geometry. They are mapped onto the 3D equilibrium, though this is not fully self-consistent. The helical core distortion may cause some level of fast ion transport and it could also modify the bootstrap current density. An accurate description of these effects requires significant modelling work with 3D transport codes that are still being validated in experiment, hence it is outside the scope of the present work.

Figure 3 shows the result of this calculation for the DIII-D V3FIT/VMEC helical core equilibrium described above. The contour plot in panels (*a*) and (*b*) represent the dynamo electrostatic potential φ. The arrows in panel (*b*) represent the associated $\mathbf{E} \times \mathbf{B}$ flow projected onto the poloidal cross section. A clear dipolar structure of the potential is observed, which corresponds to the double convective cell structure in the flow. This structure of the dynamo potential is quite similar to what is predicted by nonlinear MHD simulations, as reported for example in [37] and also found in the simulations described in next session.

An effective axisymmetric loop voltage can be calculated from the helical MHD dynamo emf using the following formula:

$$V_{\rm loop}^{\rm dyn} = \langle -\nabla\varphi \cdot \mathbf{B}\rangle / |\mathbf{B}|, \quad (4)$$

where $\langle\cdots\rangle$ represents an average over axisymmetric flux surfaces, which are obtained from the $n = 0$ Fourier component of the VMEC 3D equilibrium. The effective loop voltage obtained in this way is shown in figure 3(*c*). It is negative in the core and positive at larger radii, consistent with current broadening. The values are consistent with the effective loop voltage of -10 mV obtained from the measured poloidal flux deficit in these plasmas. It is interesting to note that the predicted helical flow is very small with values of a few m s^{-1}, consistent with the small effective loop voltage required in these plasmas. No diagnostic can measure such low rotation levels, so this quantity cannot be used to validate the MHD dynamo theory in experiment. On the other hand, it will be shown in section 4 that much higher flow values are predicted in helical RFP states, which allowed such a comparison.

The above results suggest that the MHD dynamo model is a good candidate to explain flux pumping in hybrid plasmas

with a helical core. They also show that MHD dynamo can produce enough flux pumping in a continuous way, with no need of transient events.

In more standard hybrid plasmas, flux pumping is produced by a 3/2 tearing mode. Similar calculations of the MHD dynamo emf produced by the 3/2 mode are possible, though experimental reconstructions of a 3D equilibrium with a magnetic island are not yet available. Nevertheless 3D equilibrium codes that correctly treat islands and stochastic regions are available [45] and already used to produce experimental-like equilibria [46]. In principle, such codes could be interfaced with V3FIT or similar tools to provide an experimental 3D equilibrium fit. This would require significant code development work and computational resources, but it could represent an important step to understand flux pumping in hybrid plasmas and in general the role of the MHD dynamo emf in the formation of a 3D equilibrium.

The importance of effects beyond single-fluid MHD in the saturation of helical states was recently studied with the nonlinear MHD code NIMROD [47, 48]. Such effects were introduced as first-order finite-Larmor-radius corrections to the NIMROD fluid model, including two-fluid terms in Ohm's law and ion gyroviscosity in the momentum equation. The study focused on pinch configurations, but similar effects can be expected in tokamaks. Ion gyroviscosity is found to significantly affect the saturated mode amplitude in the warm-ion case relevant to experiment. It is interesting to note that, once the saturated mode amplitude is given, for example in the present work it is obtained from experimental data, two-fluid terms do not enter the calculation of the dynamo electrostatic potential using Ohm's law, as shown with an analytic argument in [33] (see in particular paragraph 2.1.2). This justifies our approach to calculate the electrostatic potential.

3. Continuous MHD dynamo in nonlinear MHD simulations of tokamak and RFP helical states

As said above, the role of the dynamo electrostatic potential was elucidated for the first time by nonlinear MHD simulations of helical RFP states [31–33]. More recently this effect was discussed for simulations of hybrid-like high-β tokamak plasmas [37]. Here we present a comparison of nonlinear MHD simulations of tokamak and RFP helical states using the visco-resistive nonlinear MHD code SpeCyl [49]. The outputs of these simulations are analyzed with an approach similar to that used in experiment, so that experimental and modelling results can be more directly compared. The aim is to show that nonlinear MHD simulations make predictions qualitatively consistent with experiment and also to discuss similarities between helical states in tokamak and RFP. A quantitative comparison with experiment is still outside the scope of this work, due to various simplifications present in the simulations.

Since the aim of this comparison is to highlight the basic and common physics mechanisms of MHD dynamo, for simplicity the simulations have zero pressure and axisymmetric flow and are run in cylindrical geometry. The Lundquist number $S = \tau_R/\tau_A = 10^5$, where τ_R is the resistive diffusion

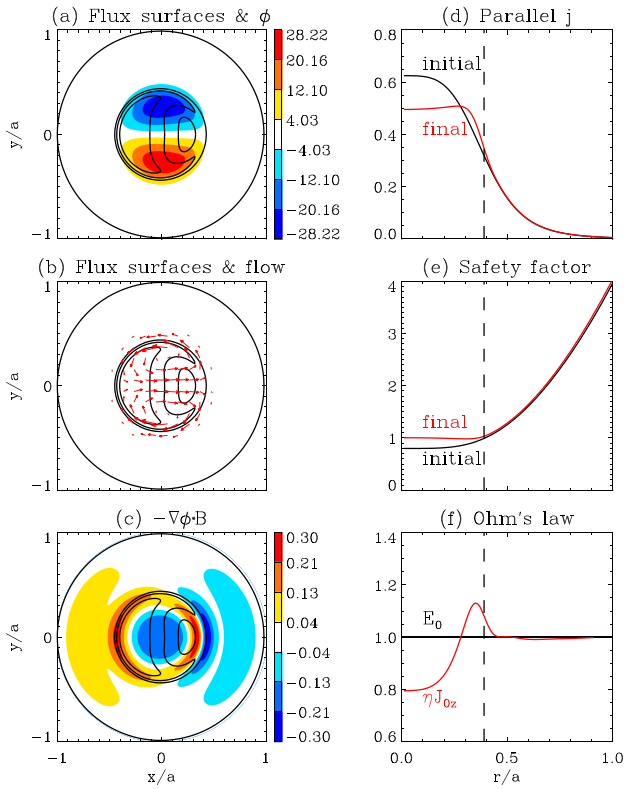

Figure 4. Results of a nonlinear MHD simulation by the SpeCyl code, in which a 1/1 mode saturates into a stationary helical equilibrium in presence of an external 1/1 field. (*a*) Helical flux surfaces (black contour levels) and dynamo electrostatic potential (color contour) during the 1/1 mode saturated phase. (*b*) Associated helical $\mathbf{E} \times \mathbf{B}$ flow (arrows). (*c*) Parallel dynamo electric field (color contour). Radial profiles of (*d*) current density, (*e*) safety factor before and after the 1/1 saturation. Panel (*f*) shows the Ohm's law terms for the final helical equilibrium. In all panels the electrostatic potential and all Ohm's law terms are normalized to the applied electric field E_0.

time and τ_A the Alfvén time, and the magnetic Prandtl number $P = \tau_V/\tau_R = 30$, where τ_V is the viscous time. In the case shown in figure 4, a 1/1 mode saturates nonlinearly in presence of an external 1/1 radial field imposed at the boundary. Without the external field, the 1/1 mode would have a sawtooth-like dynamics. Panel (*a*) shows the helical flux surfaces and the electrostatic potential, which has a dipolar structure that resembles the one calculated for DIII-D and shown in previous section. Similarly the flow in panel (*b*) shows the double convective cell pattern. The dynamo electric field parallel to the total magnetic field is shown in panel (*c*). This has a strong axisymmetric component, which is negative in the core and thus tends to limit central current peaking.

The effect of the saturated 1/1 mode on the current density profile can be better appreciated by averaging this quantity over axisymmetric flux surfaces before and after the saturation of the 1/1 mode, as shown respectively in black and red in panel (*d*). Central current is significantly redistributed and as a result the central safety factor, shown in panel (*e*), is elevated to values very close or even above unity, depending on the amplitude of the 1/1 helical deformation. This situation resembles what was found in hybrid tokamak plasmas.

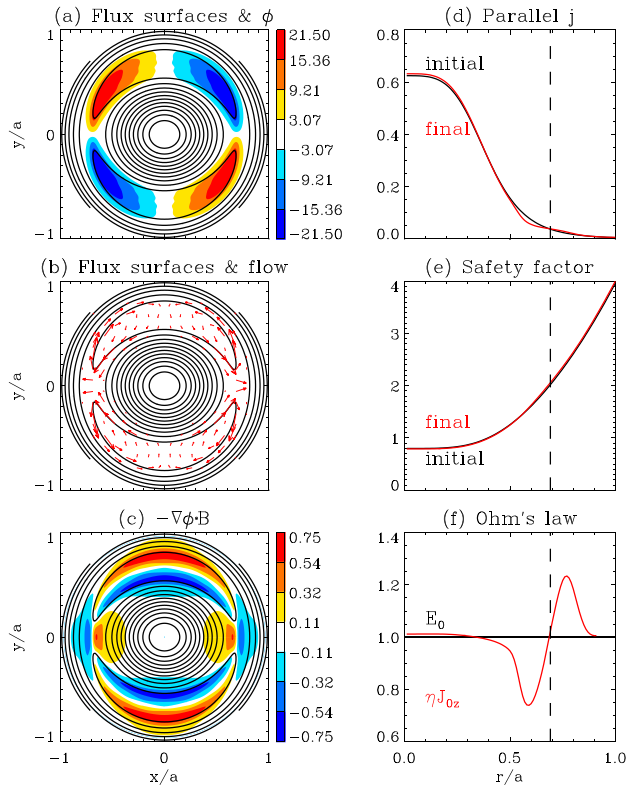

Figure 5. Same quantities described in figure 4 for a nonlinear MHD simulation by the SpeCyl code, in which a 2/1 tearing mode stimulated by an externally applied 2/1 field saturates into a stationary helical equilibrium. The simulation started from the same equilibrium used in the simulation of figure 4.

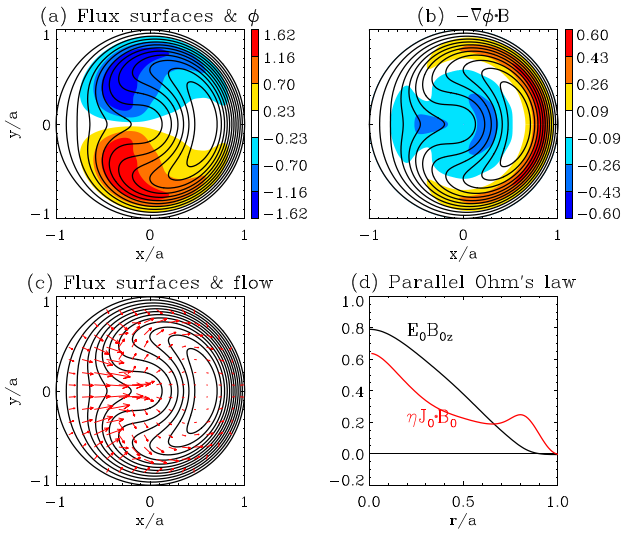

Figure 6. (*a*) Electrostatic potential, (*b*) parallel electric field, (*c*) flow, and (*d*) terms in parallel Ohm's law for a helical RFP equilibrium resulting from the spontaneous saturation of a 1/8 kink-tearing mode in a SpeCyl nonlinear MHD simulation.

The different terms in Ohm's law are shown in panel (*f*) for the final helical state. The effective dynamo loop voltage is defined in the same way as for the DIII-D calculations of previous section and has a qualitatively similar shape.

A second simulation was performed starting from the same 1D initial equilibrium and forcing a 2/1 tearing mode to grow and saturate by applying a finite 2/1 radial field at the boundary. The 2/1 mode would be stable for this particular equilibrium. A large 2/1 island develops and four convective cells form, as shown in figure 5. The dynamo effect produced by the 2/1 mode is evident in the radial profiles in the right column: the 2/1 mode redistributes current around its rational surface, but it does not affect current away from it, showing that the effect is localized where the helical displacements occurs. In toroidal shaped plasmas multiple harmonics can couple and the total dynamo effect will include contributions from all of them, possibly being more global. For example, the 2/1 mode can have a 1/1 core sideband due to finite β and minimum safety factor just above unity. Similarly the 3/2 mode can have a large 2/2 sideband. This may be directly responsible for the central current redistribution observed in hybrid plasmas, as suggested also in [12].

A simulation of a helical RFP equilibrium is shown in figure 6 for comparison with the tokamak case. In this case $S = 3 \times 10^4$ and $P = 300$. The helical displacement is here much larger than in the tokamak simulations and extends to the entire plasma, but the dynamo effect is qualitatively similar. The parallel electrostatic field in panel (*b*) is also negative in the core and positive outside it. Inspection of the different terms in parallel Ohm's law shows that significant current is redistributed from the core towards the edge. Similarly to what happens in tokamaks, the dynamo emf opposes the applied loop voltage in the plasma core, but it also drives finite parallel current in the edge region, where the parallel loop voltage goes to zero. In fact in RFPs, differently than in tokamaks, the edge parallel current is mostly poloidal and thus it cannot be driven by external induction.

4. Continuous MHD dynamo in helical RFX-mod equilibria

The MHD dynamo emf has been calculated for helical RFP states observed in RFX-mod using the same approach described in section 2 for the DIII-D helical core. Also in the RFX-mod case the 3D equilibrium was reconstructed with V3FIT/VMEC, as described in [50]. Electron temperature profiles measured by a Thomson scattering diagnostic were used as internal constraints for the reconstruction.

A typical RFX-mod discharge that exhibits spontaneous transitions to QSH is described in figure 7. QSH states occur spontaneously as the plasma current is raised above 0.8–1 MA, while a broad spectrum of $m = 1$ tearing modes is typically present at lower currents. The probability and duration of QSH states also increases continuously with plasma current. In the discharge considered here the dominant 1/7 mode has a sawtooth-like dynamics, as shown in panels (*d*) and (*e*), where its edge radial field amplitude is compared to the average amplitude of the secondary $m = 1/n > 7$ modes. But in other cases long-lasting QSH states were also observed. When the 1/7 mode is dominant, a hot helical core is observed by Thomson scattering, as reported in various papers (see [19] and references therein). The hot core region corresponds to a helically distorted electron internal transport barrier, which can extend radially up to $r/a = 0.6 - 0.7$.

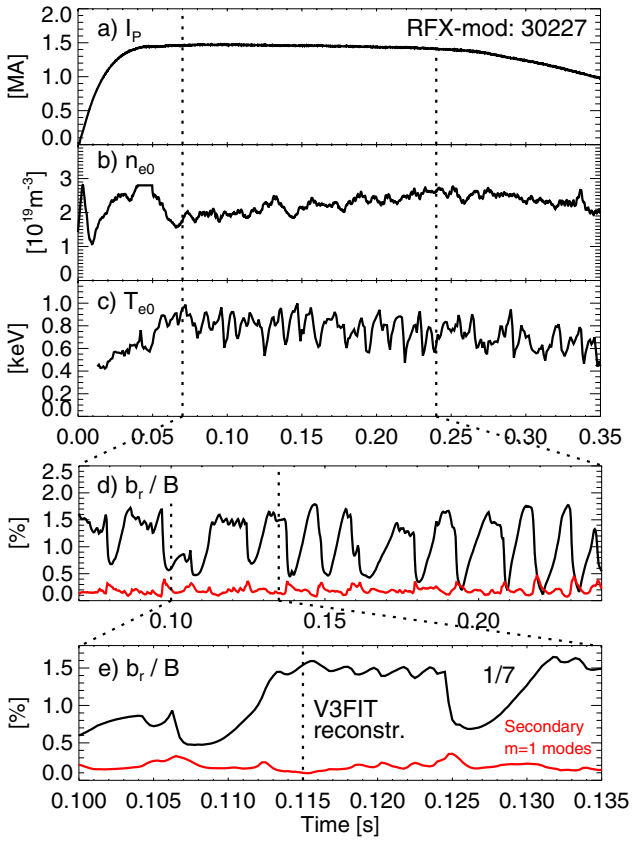

Figure 7. (*a*) Plasma current, (*b*) core electron density, (*c*) core electron temperature, and ((*d*) and (*e*)) relative B_r amplitudes of the dominant 1/7 mode (black) and average amplitude of the secondary $m = 1$, $n = 8$ to 15 modes (red) for an RFP discharge run in RFX-mod, which exhibits quasi-periodic spontaneous transitions to a QSH state followed by relaxation events. The vertical dotted line in panel (*e*) indicates the time when the helical RFP equilibrium was reconstructed by the V3FIT/VMEC code.

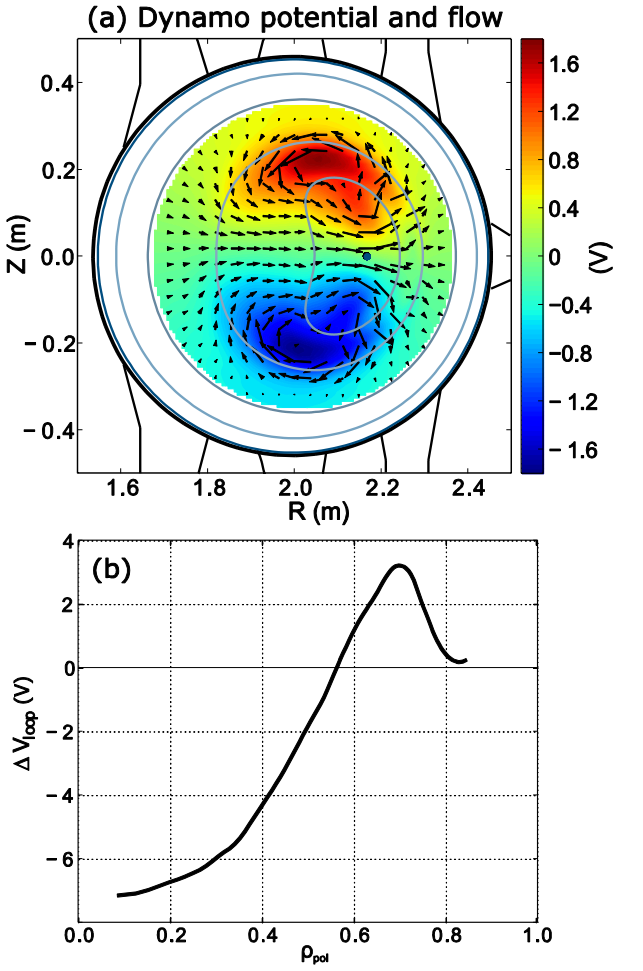

Figure 8. Calculation of the dynamo electrostatic potential for a 3D equilibrium reconstruction of a helical RFP state by the V3FIT/VMEC code for the RFX-mod discharge shown in figure 7 at $t = 0.115$ s. (*a*) The helical flux surfaces are shown with blue contours, while the color contour represents the electrostatic potential and the black arrows the associated $\mathbf{E} \times \mathbf{B}$ helical flow. (*b*) Effective dynamo loop voltage calculated as an average of the dynamo parallel electric field over axisymmetric flux surfaces, as defined in equation (4).

The helical state corresponding to the dominant 1/7 mode was reconstructed by V3FIT/VMEC for the discharge of figure 7 at $t = 0.115$ s. The resulting helical flux surfaces are shown in figure 8(*a*). The calculation of the electrostatic dynamo emf for this equilibrium followed the approach described above for DIII-D. In this case the calculation is more straightforward, since only Ohmic current drive is present and the bootstrap current fraction is negligible. The resulting electrostatic potential is represented by the color contour plot and has the expected dipolar structure similar to the DIII-D helical core. The arrows represent also in this case the associated $\mathbf{E} \times \mathbf{B}$ flow. The flow structure in the poloidal cross-section was measured in previous experiments, which found a double convective cell structure quite similar to the one predicted here [35]. Also the measured helical flow values of 1–2 km s^{-1} match pretty well this calculation.

The effective dynamo loop voltage shown in figure 8(*b*) has the expected radial profile, negative in the core and positive outside it, consistent with the required dynamo action. The negative central value of -7 V is a significant fraction of the applied loop voltage, which is around 18 V in these plasmas. These values are of course much larger than in the DIII-D hybrid plasmas, the resistivity being much larger in the RFP case. It is interesting to note that, since the magnetic field perturbation due to the 1/7 mode is similar to that of the 1/1 helical core in DIII-D, the dynamo helical flow must be larger to produce a comparably larger effective loop voltage. As a consequence, the helical flow pattern can be directly measured in RFX-mod, while the flow expected in DIII-D is too low to be detected by any available diagnostic, as said in section 2.

5. Conclusions and future work

The present work has investigated the possible role of the MHD dynamo effect in redistributing the current density profile in fusion plasmas with helical distortions due to different types of MHD modes. These included both high-β hybrid tokamak plasmas with a helical core induced by external 3D fields and high-current RFP plasmas where spontaneous transitions to helical states occur.

The main prediction of the MHD dynamo theory for these plasmas is that the dynamo mechanism can work in a continuous way in a stationary helical state. This implies that time dependent modulations of the mode amplitude are not necessary to provide the required flux pumping, which is quite promising for example in view of hybrid tokamak operation in a fusion reactor, where transient events like ELMs should be suppressed.

A new approach to calculate the dynamo electrostatic field was developed, which was made possible by the recent availability of experimental reconstructions of the 3D equilibrium by the V3FIT/VMEC code, both in DIII-D hybrid plasmas and in RFP helical states. This approach is relatively simple, though some approximations had to be made related to the effect of helical distortions on fast ion transport and on the bootstrap current. These could be avoided by more sophisticated modelling of these effects that may be performed in future work. Moreover such approximations are not necessary in RFP plasmas, which offer a quite useful test bed to validate MHD dynamo theory.

The results obtained in both tokamak and RFP plasmas are consistent with predictions of the MHD dynamo theory, though a quantitative validation is still not possible, mainly due to the above mentioned approximations. More work is also needed in the tokamak case to extend the MHD dynamo calculations to the standard situation where a 3/2 tearing mode provides flux pumping. This should be feasible by coupling V3FIT with a 3D equilibrium code that can treat magnetic islands. Such codes are available but coupling them with V3FIT still needs significant work. Substantial effort is also being spent to model these plasmas with nonlinear MHD codes complete enough as to enable quantitative predictions. This is an ongoing effort and will probably be able to provide useful results soon. Validating both approaches in present experiments is important to make robust predictions of MHD dynamo effects in future fusion machines, an important step to understand and extrapolate the hybrid tokamak scenario.

AQ4 ## Acknowledgments

This work has been carried out within the framework of the EUROfusion Consortium and has received funding from the Euratom research and training programme 2014–2018 under grant agreement No 633053. The views and opinions expressed herein do not necessarily reflect those of the European Commission. This material is based upon work supported in part by the U.S. Department of Energy, Office of Science, Office of Fusion Energy Sciences, using the DIII-D National Fusion Facility, a DOE Office of Science user facility, under awards DE-FC02-04ER54698, DE-AC05-00OR22725, DE-AC05-06OR23100, DE-FG02-04ER54761, and DE-AC52-07NA27344. DIII-D data shown in this paper can be obtained in digital format by following the links at AQ5 https://fusion.gat.com/global/D3D_DMP

References AQ6

[1] Luce T.C. *et al* 2001 *Nucl. Fusion* **41** 1585
[2] Sips A.C.C *et al* 2002 *Plasma Phys. Control. Fusion* **44** B69
[3] Joffrin E. *et al* 2003 *Plasma Phys. Control. Fusion* **45** A367
[4] Gruber O. *et al* 2009 *Nucl. Fusion* **49** 115014
[5] Oyama N. *et al* 2009 *Nucl. Fusion* **49** 065026
[6] Luce T.C. *et al* 2014 *Nucl. Fusion* **54** 013015
[7] Petty C.C. *et al* 2009 *Phys. Rev. Lett.* **102** 045005
[8] Staebler A. *et al* 2005 *Nucl. Fusion* **45** 617
[9] Stober J. *et al* 2007 *Nucl. Fusion* **47** 728
[10] Turco F. *et al* 2015 *Phys. Plasmas* **22** 056113
[11] Petty C.C. *et al* 2016 *Nucl. Fusion* **56** 016016
[12] Politzer P.A. *et al* 2005 *Proc. of the 32nd European Conf. on Plasma Physics (Tarragona) vol* 29C p 1.001–
[13] Chu M.S. *et al* 2007 *Nucl. Fusion* **47** 434
[14] Casper T.A. *et al* 2007 *Nucl. Fusion* **47** 825
[15] Piovesan P. *et al* 2017 *Plasma Phys. Control. Fusion* **59** 014027
[16] Cooper W.A. *et al* 2013 *Nucl. Fusion* **53** 073021
[17] Brunetti D. *et al* 2014 *Nucl. Fusion* **54** 064017
[18] Pfefferlé D. *et al* 2015 *Nucl. Fusion* **55** 012001
[19] Lorenzini R. *et al* 2009 *Nat. Phys.* **5** 570
[20] Piovesan P. *et al* 2013 *Phys. Plasmas* **20** 056112
[21] Moffat H.K. 1978 *Magnetic Field Generation in Electrically Conducting Fluids* (Cambridge: Cambridge University Press)
[22] Parker E.N. 1979 *Cosmical Magnetic Fields: Their Origin and Their Activity* (Oxford: Clarendon)
[23] Rüdiger G. and Hollerbach R. 2004 *The Magnetic Universe: Geophysical and Astrophysical Dynamo Theory* (Weinheim: Wiley)
[24] Ortolani S. and Schnack D.D. 1993 *Magnetohydrodynamics of Plasma Relaxation* (Singapore: World Scientific)
[25] Ji H. *et al* 1994 *Phys. Rev. Lett.* **73** 668
[26] Den Hartog D.J. *et al* 1999 *Phys. Plasmas* **6** 1813
[27] Fontana P.W. *et al* 2000 *Phys. Rev. Lett.* **85** 566
[28] Ennis D.A. *et al* 2010 *Phys. Plasmas* **17** 082102
[29] Bellan P.M. 2000 *Spheromaks: a Practical Application of Magnetohydrodynamic Dynamos and Plasma Self-Organization* (London: Imperial College Press)
[30] Hsu S.C. and Bellan P.M. 2003 *Phys. Rev. Lett.* **90** 215002
[31] Bonfiglio D. *et al* 2005 *Phys. Rev. Lett.* **94** 145001
[32] Cappello S. *et al* 2005 *Phys. Plasmas* **13** 056102
[33] Cappello S. *et al* 2011 *Nucl. Fusion* **51** 103012
[34] Piovesan P. *et al* 2004 *Phys. Rev. Lett.* **93** 235001
[35] Bonomo F. *et al* 2011 *Nucl. Fusion* **51** 123007
[36] Escande D.F. and Ottaviani M. *Phys. Lett.* A **323** 278 AQ8
[37] Jardin S.C. *et al* 2015 *Phys. Rev. Lett.* **115** 215001
[38] Hanson J.D. *et al* 2009 *Nucl. Fusion* **49** 075031
[39] Wingen A. *et al* 2017 *Nucl. Fusion* **57** 016013
[40] Cianciosa M. *et al* paper in preparation AQ9
[41] St. John H.E. *et al* 1995 *Proc. of 15th IAEA Fusion Energy Conf. on Plasma Physics and Controlled Nuclear Fusion Research (IAEA, Vienna)* vol 3 p 60
[42] Wade M.R. *et al* 2005 *Nucl. Fusion* **45** 407
[43] Luce T.C. *et al* 2014 *Nucl. Fusion* **54** 093005
[44] Taylor N.Z. *et al* paper in preparation
[45] Hirshman S.P. *et al* 2011 *Phys. Plasmas* **18** 062504
[46] Hirshman S.P. *et al* 2016 *J. Plasma Phys.* **82** 905820202
[47] King J.R. *et al* 2011 *Phys. Plasmas* **18** 042303
[48] King J.R. *et al* 2012 *Phys. Plasmas* **19** 055905
[49] Cappello S. and Paccagnella R. 1992 *Phys. Fluids* B **4** 611
[50] Terranova D. *et al* 2013 *Nucl. Fusion* **53** 113014